


PHYSICS

Coexistence of plastic and partially diffusive phases in a helium-methane compound

Hao Gao¹, Cong Liu¹, Andreas Hermann², Richard J. Needs³, Chris J. Pickard^{4,5}, Hui-Tian Wang¹, Dingyu Xing¹ and Jian Sun ^{1,*}

¹National Laboratory of Solid State Microstructures, School of Physics and Collaborative Innovation Center of Advanced Microstructures, Nanjing University, Nanjing 210093, China; ²Centre for Science at Extreme Conditions and The School of Physics and Astronomy, The University of Edinburgh, Edinburgh EH9 3FD, UK; ³Theory of Condensed Matter Group, Cavendish Laboratory, Cambridge, UK; ⁴Department of Materials Science & Metallurgy, University of Cambridge, Cambridge CB3 0HE, UK and ⁵Advanced Institute for Materials Research, Tohoku University, Sendai 980-8577, Japan

*Corresponding author. E-mail: jjiansun@nju.edu.cn

Received 29 February 2020;

Revised 5 April 2020;

Accepted 7 April 2020

ABSTRACT

Helium and methane are major components of giant icy planets and are abundant in the universe. However, helium is the most inert element in the periodic table and methane is one of the most hydrophobic molecules, thus whether they can react with each other is of fundamental importance. Here, our crystal structure searches and first-principles calculations predict that a He₃CH₄ compound is stable over a wide range of pressures from 55 to 155 GPa and a HeCH₄ compound becomes stable around 105 GPa. As nice examples of pure van der Waals crystals, the insertion of helium atoms changes the original packing of pure methane molecules and also largely hinders the polymerization of methane at higher pressures. After analyzing the diffusive properties during the melting of He₃CH₄ at high pressure and high temperature, in addition to a plastic methane phase, we have discovered an unusual phase which exhibits coexistence of diffusive helium and plastic methane. In addition, the range of the diffusive behavior within the helium-methane phase diagram is found to be much narrower compared to that of previously predicted helium-water compounds. This may be due to the weaker van der Waals interactions between methane molecules compared to those in helium-water compounds, and that the helium-methane compound melts more easily.

Keywords: crystal structure prediction, *ab initio* molecular dynamics, *ab initio* calculations, high pressure and high temperature, melting and phase transition, collective motion

INTRODUCTION

Hydrogen and helium are the most abundant elements in the universe and are significant constituents of the planets in our solar system [1]. Superionicity of hydrogen in ice and ammonia was discovered in early works [2–4]. In the superionic state, some atoms form a fixed sublattice while others diffuse as in a liquid. These states have attracted much interest in planetary and high-pressure science for some decades [5–19], because ionic mobility affects thermal and electrical conductivity deep inside planets, and therefore their thermal evolution and ability to sustain magnetic fields. For example, it has been reported that the body centered cubic (bcc) phase of superionic ice transforms to a face centered cubic (fcc) phase, which is also superionic [11]; the latter has reportedly been seen in recent shock wave experiments [18,19]. Sun *et al.* [14] reported a superionic state in close-packed and P2₁/c phases of ice at

higher pressures, and French *et al.* [15] constructed thermodynamic potentials for the superionic bcc and fcc ice phases and calculated the phase boundary between them.

Superionicity of hydrogen in ammonia and ammonia compounds has also been studied [10,12,13,16,20,21]. Methane is also an important component of giant planets in addition to water and ammonia [17]. Superionic states have not been found in methane, due to the polymerization and release of hydrogen that occurs in methane at high pressures and temperatures [22–25]. Such polymerization may result in ‘diamond rain’ in the icy planets [26]. In addition to the superionic states, the plastic phase in molecular crystals such as ammonia, in which protons rotate around the fixed nitrogen atoms, has been reported to emerge at certain pressure and temperature ranges [10]. The plastic phase and rotational motion in water have been studied

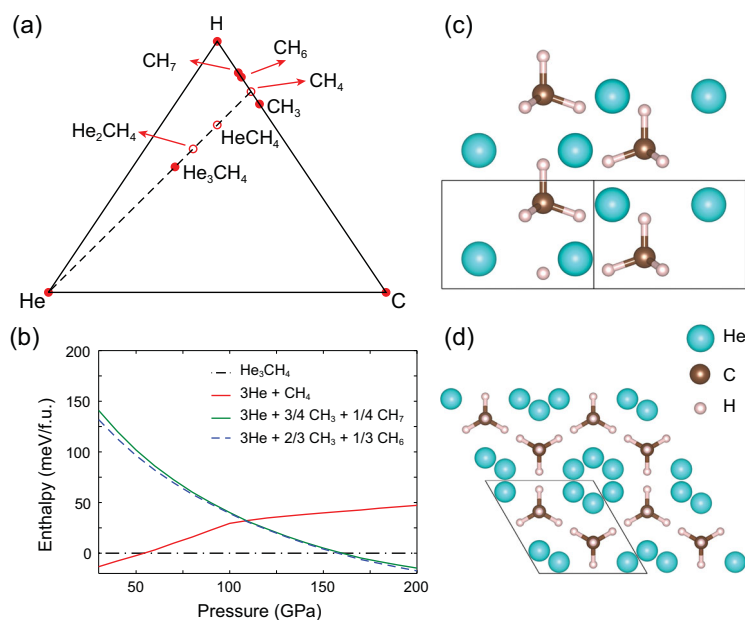


Figure 1. Energetic stability and crystal structures of He-CH₄ compounds. (a) C-H-He phase diagram at 155 GPa, (b) enthalpy-pressure relations for the C-H-He compounds and the crystal structure of He₃CH₄ viewed along [110] (c) and [001] (d). The solid and open circles represent stable and metastable phases, respectively.

under high pressure [27–29]. Very recently, Li *et al.* [30] found that colossal barocaloric effects in plastic crystals may have potential applications in solid-state refrigeration technologies.

While hydrogen-rich compounds have been studied extensively, this does not hold for helium-containing compounds. Traditionally helium is seen as the most inert element because of its closed-shell electronic configuration, but recently helium has been found to react under high pressure with metals [31,32] and ionic compounds [33–35]. Liu *et al.* [33] attributed the reactivity of helium with ionic compounds to the lowering of the Madelung energy between ions arising from the insertion of helium. At high pressures, helium has also been reported to form van der Waals (vdW) compounds with atoms such as neon [36] and covalent molecules such as ammonia [21], water [37–39], nitrogen [40–42], carbon dioxide [43] and arsenolite [44].

Superionicity involving helium has rarely been studied. Technically, helium is expected to diffuse as a neutral entity rather than an ionic entity, but a partially diffusive state involving helium has significant implications for thermal conductivities and viscosities. One such example is the helium-iron compound FeHe [32]. The superionic phase of FeHe occurs at pressures above 2 TPa and temperatures higher than 12000 K. Several superionic phases have recently been found in helium-water mixtures, which show novel behaviors such as simultaneous superionicity of hydrogen and helium [39]. However, the possi-

bility of compounds in the helium-methane system under high pressures and the nature of their high-temperature behavior are still open questions. This is despite these species forming significant portions of icy planetary atmospheres and mantles, respectively. Their miscibility is then relevant for the atmosphere-mantle boundary region, which is expected to feature large compositional gradients [45,46]. We have therefore investigated helium-methane mixtures at high pressures and temperatures.

RESULTS

In this work, searches for helium-methane compounds were performed using a machine learning accelerated crystal structure prediction method [47]. Structural optimizations, *ab initio* molecular dynamics (AIMD) simulations, enthalpies and electronic structures were calculated using the Vienna *ab initio* simulation (VASP) code [48] with projector augmented-wave potentials and the Perdew-Burke-Ernzerhof exchange-correlation functional (PBE) [49]. Further details of the calculations are provided in the Supplementary Material.

Thermodynamic stabilities of the newly predicted compounds were estimated from their relative enthalpies of formation compared with those of polymorphs of carbon, hydrogen and helium, and C–H compounds predicted in previous works [23,25,50–52]. Using an optB88-vdW functional [53,54] and hard pseudopotentials, we predicted that a new structure with a helium-methane stoichiometry of 3:1 is stable from 55 to 155 GPa (as shown in Fig. 1(a)) which is much wider than the stable pressure region of pure methane molecular crystals. Because methane decomposes above 100 GPa, here we showed a C-H-He phase diagram rather than a He-CH₄ phase diagram. The formation energy of the compound is about 32 meV/f.u. at 110 GPa (Fig. 1(b)). We have also computed the enthalpy-pressure relations using the PBE and PBE + D3 functionals [55], as shown in the Supplementary Material, all of the results confirmed that He₃CH₄ is energetically stable. He₃CH₄ is a molecular crystal with hexagonal space group (SG) *P6₃mc* composed of helium and methane molecules. As shown in Fig. 1(c) and (d), helium chains are inserted into the open channels formed by the methane molecules. The packing of methane molecules in He₃CH₄ is the same as in the experimental hexagonal closed packed (HCP) methane phase at low pressure [56], which is very different from the high-pressure phases of methane with orthorhombic space groups. Another compound, HeCH₄ with SG *P2₁/c*, is stable over a narrow range of pressures around 105 GPa. In addition,

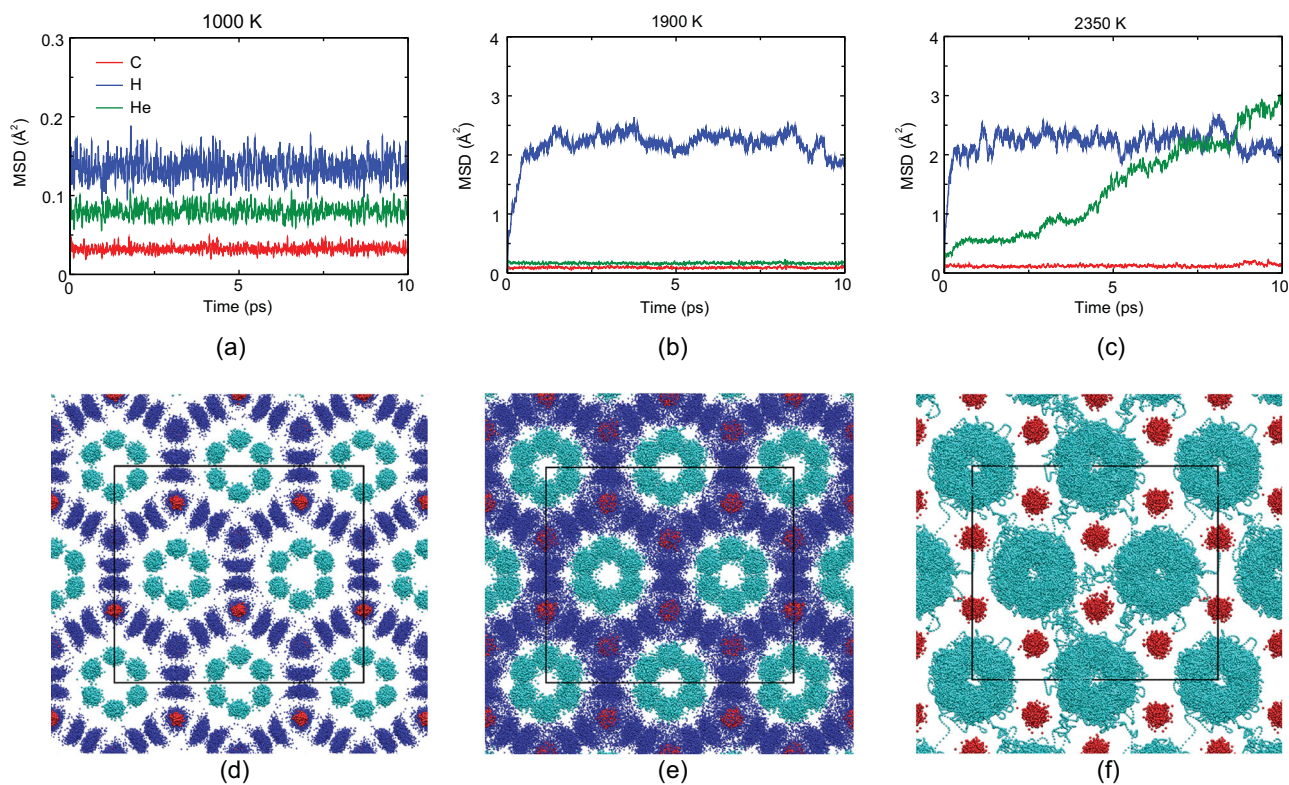


Figure 2. Dynamical behaviors of He_3CH_4 at high pressure from AIMD simulations at 1000 K, 1900 K and 2350 K. (a-c) The averaged MSD of H, He and C atoms at different temperatures. (d-f) Representations of trajectories at different temperatures in the last 10 ps. Blue, cyan and red dots represent H, He and C atoms, respectively. At 2350 K, the trajectories of H and He atoms overlap with one another, and therefore we only show He and C trajectories here.

we have also found several metastable compounds, including HeCH_4 with SG $P2_1$, He_2CH_4 with SG $P3_1m$ and $P2_1/m$, and $\text{He}_2(\text{CH}_4)_3$ with SG Cm . These metastable phases are very close to the convex hull. The phase diagrams under different pressures are shown in the Supplementary Material.

He_3CH_4 is an insulator with a large band gap of 8.9 eV at 50 GPa, as shown in Fig. S11 in the Supplementary Material, it is higher than that of pure methane molecular crystals. The phonon band structures of He_3CH_4 at 0 and 50 GPa shown in the Supplementary Material indicate the dynamical stability of this compound. HeCH_4 is also found to be an insulator with a large band gap and is dynamically stable. The conditions in the upper mantle regions of icy planets reach tens to hundreds of GPa and thousands of K [45]. To obtain the dynamical properties of He_3CH_4 we performed AIMD simulations within the pressure range 50–200 GPa and the temperature range 500–3000 K. The averaged mean squared displacements (MSD) of hydrogen, helium and carbon atoms were calculated to study phase transitions induced by temperature and pressure. According to the diffusive behaviors of the different atoms, the states of He_3CH_4 can be divided into four types: the solid phase, a plastic CH_4

phase, a phase of plastic CH_4 plus diffusive He, and the fluid phase.

We used three representative trajectories to reveal the differences between the states by comparing their MSD and motions, as shown in Fig. 2. All of the simulations start from the relaxed configuration at 150 GPa, which are independent, but with different temperatures. At 1000 K, the atoms are restricted to their equilibrium positions, and exhibit small vibrations. As shown in Fig. 2(a), the MSD of the atoms are extremely small in the simulations, thus He_3CH_4 remains in the solid phase at this temperature.

When the temperature increases to 1900 K, the compound transforms to the plastic CH_4 phase. As shown in Fig. 2(b), the averaged MSD of H atoms increases rapidly in a short timescale, and stays about 2.0 \AA^2 afterwards. This is deemed to be a plastic phase when the methane molecules are free to rotate around the carbon atoms with small fluctuations of C-H bond lengths and angles (Fig. 2(e)). Plastic phases have also been reported in pure methane [57], ice [27,58], ammonia [10,12] and helium-ammonia compounds [21]. Meanwhile, the averaged MSD values of He and C atoms are still very small. Using the rigid molecule approximation [57] we have been able to calculate the

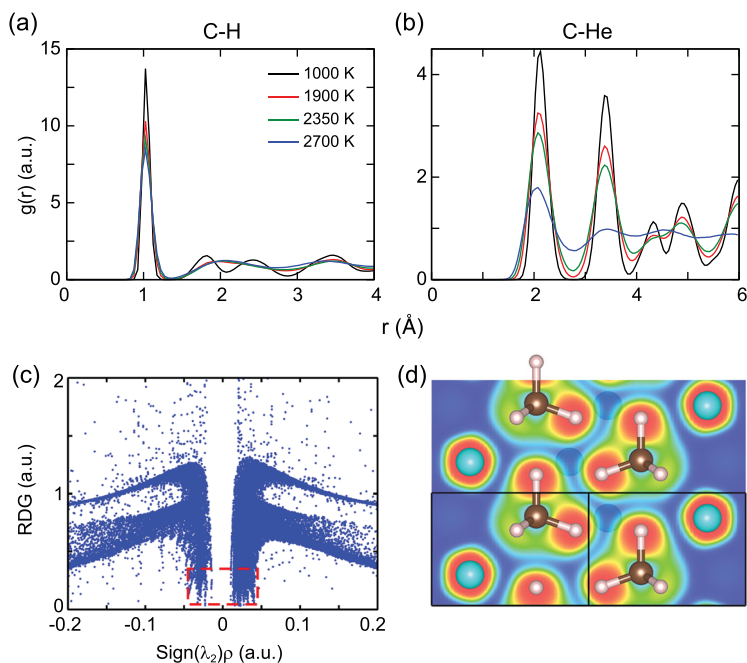


Figure 3. Dynamical structure and interaction analysis. Radial distribution functions (RDFs) for C-H (a) and C-He (b) pairs in He_3CH_4 at around 150 GPa and heating to about 1000 K (solid phase), 1900 K (plastic phase), 2350 K (coexistence of plastic and partially diffusive phase) and 2700 K (fluid phase). (c) Plots of the reduce density gradient (RDG) versus the electron density multiplied by the sign of the second largest eigenvalue of the electron-density Hessian matrix. (d) ELF plotted in the (110) plane.

theoretical MSD of the H atoms. Suppose that the methane molecules are rigid with fixed radius r_{CH} (the length of a C-H bond). For one of the H atoms, its initial position is $\mathbf{r}_0(r_{\text{CH}}, 0, 0)$ in spherical coordinates. Since methane molecules rotate freely, the position of the H atom $\mathbf{r}(r_{\text{CH}}, \theta, \phi)$ is distributed uniformly over the sphere of radius r_{CH} . Therefore, the analytical MSD is

$$\begin{aligned} \langle (r - r_0)^2 \rangle &= \frac{1}{4\pi} \int_0^\pi d\theta \int_0^{2\pi} d\phi \sin\theta (r - r_0^2) \\ &= \frac{2r_{\text{CH}}^2}{4\pi} \int_0^\pi d\theta \int_0^{2\pi} d\phi \sin\theta \\ &\quad \times (1 - \cos\theta) = 2r_{\text{CH}}^2. \end{aligned} \quad (1)$$

For the plastic CH_4 phase, the resulting MSD is $\langle (r - r_0)^2 \rangle = 2.142 \text{ \AA}^2$, which is very close to the value from our AIMD calculations (2.169 \AA^2).

At higher temperatures (2350 K) methane molecules rotate while helium atoms are diffusive (Fig. 2(c) and (f)), which leads to the formation of a superionic-like He state in He_3CH_4 . The diffusion coefficient of helium atoms D_{He} is $4.81 \times 10^{-10} \text{ m}^2/\text{s}$ from the velocity auto-correlation functions (VACFs). We obtain very similar results $D_{\text{He}} = 4.48 \times 10^{-10} \text{ m}^2/\text{s}$ from the MSD. Diffusion coefficients of helium along different directions were also calcu-

lated: $D_{\text{He}}^x = 3.79 \times 10^{-10} \text{ m}^2/\text{s}$, $D_{\text{He}}^y = 4.02 \times 10^{-10} \text{ m}^2/\text{s}$, $D_{\text{He}}^z = 6.62 \times 10^{-10} \text{ m}^2/\text{s}$. The existence of open channels along the z axis in He_3CH_4 (Fig. 1(d)) can explain the anisotropy of diffusion coefficients. Heating the superionic phases of He_3CH_4 eventually leads to melting of the methane sublattice, which gives rise to the fluid phase.

We can further understand the dynamical processes of the He_3CH_4 structure at different temperatures by using the radial distribution function (RDF). C-H and C-He partial RDFs are shown in Fig. 3(a) and (b) and others are shown in the Supplementary Material. The C-He, He-He and H-He partial RDFs of the partially diffusive phase (2350 K, green lines) are very similar to those of the plastic phase (1900 K, red lines), but are clearly different to those of the fluid phase (2700 K, blue lines). We analyzed some trajectories of the partially diffusive phase and found that the diffusion of helium atoms maintains the order of the helium chains. In some cases of the partially diffusive phase we can see the plateaus in the averaged MSD of He. The performance of the diffusive helium atoms is similar to collective diffusion of ions in lithium battery cathode materials [59,60]. The atoms jump along the chains or hop from one chain to another and therefore the RDFs remain solid-like. However, in the fluid phase, the sublattices of helium and methane have already melted and the RDFs are liquid-like. Finally, the first peak of the C-H RDFs remains essentially unchanged deep into the fluid phase. This indicates that the integrity of the methane molecules is maintained up to the highest temperature.

The superionic state in helium-methane differs from the few other examples of superionic helium [32,39] because plastic CH_4 and diffusive He states coexist. Plastic and superionic phases also appear in the phase diagram of ammonia and ice [10,12,58], but they cannot coexist since both the plastic and diffusive atoms in ammonia and water are protons.

From the results of extensive AIMD simulations, we proposed a phase diagram of He_3CH_4 between 50 and 200 GPa and below 3000 K (Fig. 4). The colored dots represent independent NVT (Canonical Ensemble) simulations which are classified by their averaged MSDs and RDFs (tests with the NPT (Isothermal-Isobaric Ensemble) confirm these classifications, see the Supplementary Material). The phase boundaries divide the diagram into four regions: solid, plastic CH_4 , plastic CH_4 + diffusive He and fluid phases. The partially diffusive phase appears at pressures above 70 GPa within a narrow range. Compared with helium-water compounds, He_3CH_4 is dominated by dispersion interactions between methane molecules, which are much weaker than the

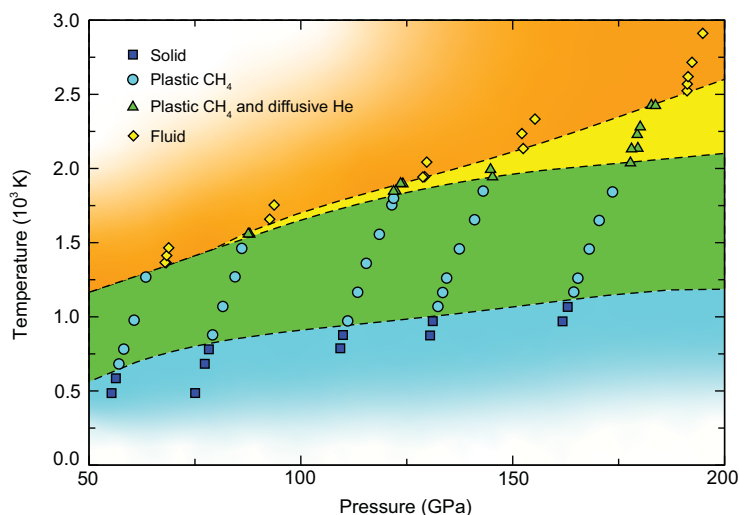


Figure 4. Phase diagram of He_3CH_4 as determined in this work. Each symbol represents an AIMD simulation. The dashed lines are phase boundaries.

hydrogen bonds between water molecules. Therefore the ice frameworks in helium-water compounds are more stable than the sublattice of methane molecules. There are many open channels in helium-water compounds, which results in a much wider partially diffusive region in helium-water than that in the helium-methane system. To validate the superionicity of helium we have performed AIMD calculations at 150 GPa using hard pseudopotentials. The results are shown in the Supplementary Material and the appearance of the partially diffusive phase at high temperatures is unaffected.

To investigate the interactions in He_3CH_4 we have applied a real-space analysis to the helium-methane compound. According to the electron localization function (ELF) shown in Fig. 3(d), strong intramolecular covalent bonds persist between carbon and hydrogen atoms while the interactions between methane and helium molecules are of closed-shell character. The types of intermolecular interactions in He_3CH_4 can be determined using the atoms-in-molecules (AIM) theory [61] and reduced density gradient (RDG) analysis [62]. Based on AIM, a topological analysis of the electron density $\rho(\mathbf{r})$ was carried out to compute atomic Bader charges and search for bond critical points (BCPs). We found that the charge transfer in He_3CH_4 is less than $0.03e$ between carbon and hydrogen. This is consistent with the fact that the electronegativities of carbon and hydrogen are similar and methane cannot participate in hydrogen bonding. A BCP connecting a pair of atoms provides important information about the bonding between atoms. We show all of the non-equivalent BCPs and their properties in the Supplementary Material. The first and

second BCPs represent the bonds inside methane molecules. The electron densities at these BCPs are much larger than others and the negative Laplacian values indicate the concentration of electrons between the carbon and hydrogen atoms. These are typical features of covalent bonding. Other BCPs with small densities and positive Laplacian values are characteristic of dispersion interactions. Furthermore, reduced density gradient analysis has been applied to the electron density. As shown in Fig. 3(c), the spikes at low density, the low-gradient region (inside the red dashed box) reflects the existence of non-covalent interactions [62] in He_3CH_4 . The distinct spikes are very near zero, indicating that the type is vdW interactions, which are weaker than hydrogen bonds in helium-water [39] and helium-ammonia compounds [21].

DISCUSSION

The isotopic effects in hydrogen are important in some cases [63] and we have accounted for them in the helium-methane compound by comparing the vibrational densities of states (VDOS) of He_3CH_4 and He_3CD_4 (Supplementary Material). Within the harmonic approximation, isotopic effects lead to changes in the atomic mass and in the phonon frequencies. The frequency of the highest peak in the partial VDOS drops from about 3700 cm^{-1} for hydrogen to about 2700 cm^{-1} for deuterium, with a ratio of about $1/\sqrt{2}$. Since strong covalent bonds exist between carbon and hydrogen/deuterium, the highest phonon peaks of carbon have the same tendencies as the isotopic effects. In contrast, the frequency region of the helium VDOS does not change substantially, because the vdW interactions between helium and methane are weak. The isotopic effects can also influence dynamical properties, and therefore we conducted AIMD calculations for He_3CD_4 at 2350 K and compared the VDOS of He_3CH_4 and He_3CD_4 at high temperatures. For carbon and hydrogen/deuterium the reduction of the frequencies also appears with the ratio of $1/\sqrt{2}$. For helium, the partial VDOS is very similar. This demonstrates that isotopic effects do not substantially affect the superionicity of the helium-methane compound.

In previous studies nuclear quantum effects were considered for ice [15] and mixtures of methane, ammonia and water [64]. The nuclear quantum corrections for He_3CH_4 at different densities and temperatures are shown in the Supplementary Material. The quantum corrections for the helium-methane compounds are slightly larger than those for ice [15] because of the higher proportion of hydrogen and

helium in the compound and the lower temperature region in our simulations.

CONCLUSION

In summary, we have predicted a helium-methane compound (He_3CH_4) that is stable at pressures relevant to upper mantle conditions of icy planets. The inclusion of He atoms highly changes the packing of methane molecules and the stable pressure region of the helium-methane compound is much wider than that of pure methane. He insertion also changes the electronic properties of methane. For example, the band gap of He_3CH_4 is larger than that of pure methane. Moreover, the phase diagram of He_3CH_4 has been investigated and a novel phase of coexistence of plastic methane and diffusive helium has been found. The temperature range of the partially diffusive regime in helium-methane is narrower than that in the helium-water system, due to the weaker interactions between the methane molecules, which results in a relatively fragile framework and an easier transition to the fluid state than in the helium-water system. In addition, we observed anisotropy in the He diffusion, which is related to the structure of the compound. We have also analyzed the interactions in He_3CH_4 and their effects on the phase diagram in comparison with previously predicted helium-water compounds. This work should be helpful in constructing models of icy giant planets, and it would be very instructive to investigate how much the finite-temperature miscibility of helium and methane reflects our ground state results [65].

METHODS

We used a Bayesian-Optimization-based crystal structure prediction method [47] combined with VASP to predict new compounds for the He- CH_4 system. The prediction results have been checked by *ab initio* random structure searching (AIRSS) [66]. The optB88-vdW functional [53] was employed to account for vdW interactions in the calculations of enthalpies and electronic structures. A basis set energy cutoff of 720 eV was used except for the AIMD calculations, for which a lower cutoff energy of 625 eV was used for reducing the computational cost of extensive AIMD simulations. The Brillouin zone was sampled with a Monkhorst-Pack k-point mesh with a spacing of $2\pi \times 0.03 \text{ \AA}^{-1}$. The phonon dispersion curves were calculated using $2 \times 2 \times 2$ supercells with PHONOPY code [67] to validate the dynamical stabilities of the predicted structures. The AIM [61] and RDG [62] analysis of the electron density $\rho(r)$ was performed using the

critic2 code [68]. We used orthorhombic supercells containing 256 atoms to perform AIMD simulations for He_3CH_4 in the NVT ensemble with Γ -centered k-points sampling. The time step of AIMD was set to 1 fs and all simulations were carried out with at least 3000 steps. Some trajectories were extended to more than 10 ps to confirm the stabilities. In addition, to validate our results we employed hard pseudopotentials for hydrogen and carbon and repeated the calculations. The cutoff energy of 1000 eV was used to calculate pressure-composition phase diagrams. A cutoff energy of 910 eV was used for the AIMD simulations. The nuclear quantum corrections of free energies are calculated from the AIMD trajectories using the method proposed in reference [15].

SUPPLEMENTARY DATA

Supplementary data are available at [NSR](https://doi.org/10.1039/C9CP00000A) online.

ACKNOWLEDGEMENTS

The calculations were carried out using supercomputers at the High Performance Computing Center of Collaborative Innovation Center of Advanced Microstructures, high performance supercomputing center of Nanjing University; 'Tianhe-2' at NSCC-Guangzhou; and the CSD3 Peta4 CPU/KNL machine in the University of Cambridge.

FUNDING

J.S. gratefully acknowledges financial support from the National Key R&D Program of China (2016YFA0300404), the National Natural Science Foundation of China (11974162 and 11834006), the Fundamental Research Funds for the Central Universities. C.J.P. and R.J.N. acknowledge financial support from the Engineering and Physical Sciences Research Council (EPSRC) of the U.K. under grants [EP/G007489/2] (C.J.P.) and [EP/P034616/1] (R.J.N.). C.J.P. also acknowledges financial support from EPSRC and the Royal Society through a Royal Society Wolfson Research Merit award.

AUTHOR CONTRIBUTIONS

J.S. conceived and led the project. H.G. and C.J.P. performed the calculations. J.S., H.G. and C.L. made the analysis. J.S., H.G., A.H., and R.J.N. wrote the manuscript. All authors discussed the results and commented on the manuscript.

Conflict of interest statement. None declared.

REFERENCES

1. Stevenson DJ. Metallic helium in massive planets. *Proc Natl Acad Sci USA* 2008; **105**: 11035–6.
2. Ryzhkin IA. Superionic transition in ice. *Solid State Commun* 1985; **56**: 57–60.
3. Demontis P, LeSar R and Klein ML. New high-pressure phases of ice. *Phys Rev Lett* 1988; **60**: 2284–7.

4. Cavazzoni C, Chiarotti GL and Scandolo S *et al.* Superionic and metallic states of water and ammonia at giant planet conditions. *Science* 1999; **283**: 44–6.
5. Yakushev VV, Postnov VI and Fortov VE *et al.* Electrical conductivity of water during quasi-isentropic compression to 130 GPa. *J Exp Theor Phys* 2000; **90**: 617–22.
6. Chau R, Mitchell AC and Minich RW *et al.* Electrical conductivity of water compressed dynamically to pressures of 70–180 GPa (0.7–1.8 Mbar). *J Chem Phys* 2001; **114**: 1361–5.
7. Goncharov AF, Goldman N and Fried LE *et al.* Dynamic ionization of water under extreme conditions. *Phys Rev Lett* 2005; **94**: 125508.
8. French M, Mattsson TR and Nettelmann N *et al.* Equation of state and phase diagram of water at ultrahigh pressures as in planetary interiors. *Phys Rev B* 2009; **79**: 054107.
9. Redmer R, Mattsson TR and Nettelmann N *et al.* The phase diagram of water and the magnetic fields of Uranus and Neptune. *Icarus* 2011; **211**: 798–803.
10. Ninet S, Datchi F and Saitta AM. Proton disorder and superionicity in hot dense ammonia ice. *Phys Rev Lett* 2012; **108**: 165702.
11. Wilson HF, Wong ML and Militzer B. Superionic to superionic phase change in water: consequences for the interiors of Uranus and Neptune. *Phys Rev Lett* 2013; **110**: 151102.
12. Bethkenhagen M, French M and Redmer R. Equation of state and phase diagram of ammonia at high pressures from ab initio simulations. *J Chem Phys* 2013; **138**: 234504.
13. Bethkenhagen M, Cebulla D and Redmer R *et al.* Superionic phases of the 1:1 water–ammonia mixture. *J Phys Chem A* 2015; **119**: 10582–8.
14. Sun J, Clark BK and Torquato S *et al.* The phase diagram of high-pressure superionic ice. *Nat Commun* 2015; **6**: 8156.
15. French M, Desjarlais MP and Redmer R. *Ab initio* calculation of thermodynamic potentials and entropies for superionic water. *Phys Rev E* 2016; **93**: 022140.
16. Jiang X, Wu X and Zheng Z *et al.* Ionic and superionic phases in ammonia dihydrate $\text{NH}_3 \cdot 2\text{H}_2\text{O}$ under high pressure. *Phys Rev B* 2017; **95**: 144104.
17. Bethkenhagen M, Meyer ER and Hamel S *et al.* Planetary ices and the linear mixing approximation. *Astrophys J* 2017; **848**: 67.
18. Millot M, Hamel S and Rygg JR *et al.* Experimental evidence for superionic water ice using shock compression. *Nat Phys* 2018; **14**: 297.
19. Millot M, Coppari F and Rygg JR *et al.* Nanosecond X-ray diffraction of shock-compressed superionic water ice. *Nature* 2019; **569**: 251–5.
20. Song X, Yin K and Wang Y *et al.* Exotic hydrogen bonding in compressed ammonia hydrides. *J Phys Chem Lett* 2019; **10**: 2761–6.
21. Liu C, Gao H and Hermann A *et al.* Plastic and superionic helium ammonia compounds under high pressure and high temperature. *Phys Rev X* 2020; **10**: 021007.
22. Hirai H, Konagai K and Kawamura T *et al.* Polymerization and diamond formation from melting methane and their implications in ice layer of giant planets. *Phys Earth Planet Inter* 2009; **174**: 242–6.
23. Gao G, Oganov AR and Ma Y *et al.* Dissociation of methane under high pressure. *J Chem Phys* 2010; **133**: 144508.
24. Sherman BL, Wilson HF and Weeraratne D *et al.* Ab initio simulations of hot dense methane during shock experiments. *Phys Rev B* 2012; **86**: 224113.
25. Conway LJ and Hermann A. High pressure hydrocarbons revisited: from van der Waals compounds to diamond. *Geosciences* 2019; **9**: 227.
26. Kraus D, Vorberger J and Pak A *et al.* Formation of diamonds in laser-compressed hydrocarbons at planetary interior conditions. *Nat Astronomy* 2017; **1**: 606–11.
27. Takii Y, Koga K and Tanaka H. A plastic phase of water from computer simulation. *J Chem Phys* 2008; **128**: 204501.
28. Aragoes JL and Vega C. Plastic crystal phases of simple water models. *J Chem Phys* 2009; **130**: 244504.
29. Bove LE, Klotz S and Strässle TH *et al.* Translational and rotational diffusion in water in the gigapascal range. *Phys Rev Lett* 2013; **111**: 185901.
30. Li B, Kawakita Y and Ohira-Kawamura S *et al.* Colossal barocaloric effects in plastic crystals. *Nature* 2019; **567**: 506.
31. Dong X, Oganov AR and Goncharov AF *et al.* A stable compound of helium and sodium at high pressure. *Nat Chem* 2017; **9**: 440–5.
32. Monserrat B, Martinez-Canales M and Needs RJ *et al.* Helium-iron compounds at terapascal pressures. *Phys Rev Lett* 2018; **121**: 015301.
33. Liu Z, Botana J and Hermann A *et al.* Reactivity of He with ionic compounds under high pressure. *Nat Commun* 2018; **9**: 951.
34. Zhang X, Lv J and Li H *et al.* Rare helium-bearing compound FeO_2He stabilized at deep-earth conditions. *Phys Rev Lett* 2018; **121**: 255703.
35. Gao H, Sun J and Pickard CJ *et al.* Prediction of pressure-induced stabilization of noble-gas-atom compounds with alkali oxides and alkali sulfides. *Phys Rev Mater* 2019; **3**: 015002.
36. Loubeyre P, Jean-Louis M and LeToullec R *et al.* High pressure measurements of the He-Ne binary phase diagram at 296 K: evidence for the stability of a stoichiometric $\text{Ne}(\text{He})_2$ solid. *Phys Rev Lett* 1993; **70**: 178–81.
37. Liu H, Yao Y and Klug DD. Stable structures of He and H_2O at high pressure. *Phys Rev B* 2015; **91**: 014102.
38. Teeratchanan P and Hermann A. Computational phase diagrams of noble gas hydrates under pressure. *J Chem Phys* 2015; **143**: 154507.
39. Liu C, Gao H and Wang Y *et al.* Multiple superionic states in helium–water compounds. *Nat Phys* 2019; **15**: 1065–70.
40. Vos WL, Finger LW and Hemley RJ *et al.* A high-pressure van der Waals compound in solid nitrogen-helium mixtures. *Nature* 1992; **358**: 46–8.
41. Ninet S, Weck G and Loubeyre P *et al.* Structural and vibrational properties of the van der Waals compound $(\text{N}_2)_{11}\text{He}$ up to 135 GPa. *Phys Rev B* 2011; **83**: 134107.
42. Li Y, Feng X and Liu H *et al.* Route to high-energy density polymeric nitrogen t-N via He–N compounds. *Nat Commun* 2018; **9**: 722.
43. Li D, Liu Y and Tian F *et al.* High-pressure structures of helium and carbon dioxide from first-principles calculations. *Solid State Commun* 2018; **283**: 9–13.
44. Sans JA, Manjón FJ and Popescu C *et al.* Ordered helium trapping and bonding in compressed arsenolite: synthesis of $\text{As}_4\text{O}_6 \cdot 2\text{He}$. *Phys Rev B* 2016; **93**: 054102.
45. Nettelmann N, Wang K and Fortney JJ *et al.* Uranus evolution models with simple thermal boundary layers. *Icarus* 2016; **275**: 107–16.
46. French M and Nettelmann N. Viscosity and prandtl number of warm dense water as in ice giant planets. *Astrophys J* 2019; **881**: 81.
47. Xia K, Gao H and Liu C *et al.* A novel superhard tungsten nitride predicted by machine-learning accelerated crystal structure search. *Sci Bull* 2018; **63**: 817–24.
48. Kresse G and Furthmüller J. Efficient iterative schemes for ab initio total-energy calculations using a plane-wave basis set. *Phys Rev B* 1996; **54**: 11169–86.
49. Perdew JP, Burke K and Ernzerhof M. Generalized gradient approximation made simple. *Phys Rev Lett* 1996; **77**: 3865–8.
50. Wen X-D, Hand L and Labet V *et al.* Graphane sheets and crystals under pressure. *Proc Natl Acad Sci USA* 2011; **108**: 6833–7.
51. Liu Y, Duan D and Tian F *et al.* Crystal structures and properties of the CH_4H_2 compound under high pressure. *RSC Adv* 2014; **4**: 37569–74.
52. Saleh G and Oganov AR. Novel stable compounds in the C–H–O Ternary system at high pressure. *Sci Rep* 2016; **6**: 32486.

53. Klimeš J, Bowler DR and Michaelides A. Chemical accuracy for the van der Waals density functional. *J Phys Condens Matter* 2010; **22**: 022201.
54. Dion M, Rydberg H and Schröder E *et al.* Van der Waals density functional for general geometries. *Phys Rev Lett* 2004; **92**: 246401.
55. Grimme S, Antony J and Ehrlich S *et al.* A consistent and accurate ab initio parametrization of density functional dispersion correction (DFT-D) for the 94 elements H-Pu. *J Chem Phys* 2010; **132**: 154104.
56. Bini R and Pratesi G. High-pressure infrared study of solid methane: phase diagram up to 30 GPa. *Phys Rev B* 1997; **55**: 14800–9.
57. Spanu L, Donadio D and Hohl D *et al.* Theoretical investigation of methane under pressure. *J Chem Phys* 2009; **130**: 164520.
58. Hernandez J-A and Caracas R. Proton dynamics and the phase diagram of dense water ice. *J Chem Phys* 2018; **148**: 214501.
59. He X, Zhu Y and Mo Y. Origin of fast ion diffusion in super-ionic conductors. *Nat Commun* 2017; **8**: 15893.
60. Zimmermann NER, Hannah DC and Rong Z *et al.* Electrostatic estimation of intercalant jump-diffusion barriers using finite-size ion models. *J Phys Chem Lett* 2018; **9**: 628–34.
61. Bader RFW. A quantum theory of molecular structure and its applications. *Chem Rev* 1991; **91**: 893–928.
62. Johnson ER, Keinan S and Mori-Sánchez P *et al.* Revealing noncovalent interactions. *J Am Chem Soc* 2010; **132**: 6498–506.
63. Hermann A, Ashcroft NW and Hoffmann R. Isotopic differentiation and sublattice melting in dense dynamic ice. *Phys Rev B* 2013; **88**: 214113.
64. Meyer ER, Ticknor C and Bethkenhagen M *et al.* Bonding and structure in dense multi-component molecular mixtures. *J Chem Phys* 2015; **143**: 164513.
65. Schöttler M and Redmer R. Ab initio calculation of the miscibility diagram for hydrogen-helium mixtures. *Phys Rev Lett* 2018; **120**: 115703.
66. Pickard CJ and Needs RJ. *Ab initio* random structure searching. *J Phys Condensed Matter* 2011; **23**: 053201.
67. Togo A and Tanaka I. First principles phonon calculations in materials science. *Scr Mater* 2015; **108**: 1–5.
68. Otero-de-la-Roza A, Johnson ER and Luaña V. Critic2: a program for real-space analysis of quantum chemical interactions in solids. *Comp Phys Commun* 2014; **185**: 1007–18.